

# Rhombot: Rhombus-shaped Modular Robots for Stable, Medium-Independent Reconfiguration Motion

Jie Gu<sup>1</sup>, Yirui Sun<sup>1</sup>, Zhihao Xia<sup>1</sup>, Tin Lun Lam<sup>2,3</sup>, Chunxu Tian<sup>1,†</sup>, Dan Zhang<sup>1,4,†</sup>

**Abstract**—In this paper, we present Rhombot, a novel deformable planar lattice modular self-reconfigurable robot (MSRR) with a rhombus shaped module. Each module consists of a parallelogram skeleton with a single centrally mounted actuator that enables folding and unfolding along its diagonal. The core design philosophy is to achieve essential MSRR functionalities such as morphing, docking, and locomotion with minimal control complexity. This enables a continuous and stable reconfiguration process that is independent of the surrounding medium, allowing the system to reliably form various configurations in diverse environments. To leverage the unique kinematics of Rhombot, we introduce morphpivoting, a novel motion primitive for reconfiguration that differs from advanced MSRR systems, and propose a strategy for its continuous execution. Finally, a series of physical experiments validate the module’s stable reconfiguration ability, as well as its positional and docking accuracy.

## I. INTRODUCTION

Traditional Modular Self-Reconfigurable Robots (MSRRs) are able to deploying to versatile configurations to adapt to different environment and reusable across a wide range of missions, often built with rigid modules in chain, lattice, mobile, hybrid, or freeform form [1]–[8].

With the continuous emergence of new modular robot designs, module structures are no longer confined to a single, well-defined configuration but instead exhibit multiple overlapping attributes. A detailed review of such overlapping and fuzzy classifications is provided in [9]. Different attributes offer advantages for different functional objectives; for example, modules with mobile attributes enhance locomotion capabilities [10], those with chain attributes are better suited for manipulation tasks [11], and those with lattice attributes facilitate the rapid construction of temporary structures [12].

Our work primarily focuses on MSRRs with lattice attributes. For such robots, the most common reconfiguration motion is based on the disassembly of modules through the surrounding medium. If the robotic system permits individual modules to detach, the system can, in theory, be entirely disassembled and reassembled to achieve any desired configuration. However, this approach faces a significant challenge:

\*This work was supported by the National Nature Science Foundation of China (grants 52305012).

<sup>1</sup>Institute of AI and Robotics, Academy for Engineering & Technology, Fudan University, Shanghai 200433, China.

<sup>2</sup>School of Science and Engineering, The Chinese University of Hong Kong, Shenzhen, China.

<sup>3</sup>Shenzhen Institute of Artificial Intelligence and Robotics for Society.

<sup>4</sup>Department of Mechanical Engineering, The Hong Kong Polytechnic University, Hung Hom.

<sup>†</sup>Corresponding author is Chunxu Tian, email: chxtian@fudan.edu.cn and Dan Zhang, email: dan.zhang@polyu.edu.hk

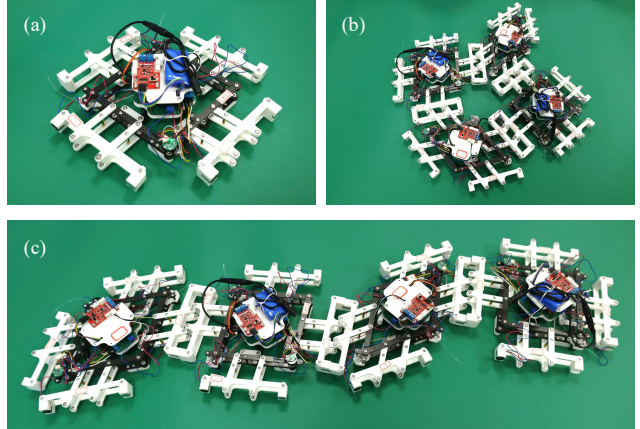


Fig. 1. Prototype of Rhombot. (a) Single Module. (b) Lattice Assembly. (c) Chain Assembly.

each module must precisely determine its designated position and successfully complete accurate docking. Another reconfiguration method is independent of the surrounding medium, relying instead on pivoting [13], [14] or on the module’s intrinsic deformation capability to move toward neighboring voids [15]–[17]. The former approach imposes strict requirements on landing accuracy and does not allow modules to maintain intermediate states during transformation. In contrast, deformation-based approaches provide more stable connections and can maintain arbitrary intermediate configurations at any time.

In modular robots with deformable modules, modules are always interconnected through edges/faces in 2D/3D configurations [18], [19]. During reconfiguration, the system ensures that every module remains connected to the overall structure through at least one edge or face, enabling stable and continuous reconfiguration motions. Furthermore, the relative coordinate frames defined within the system allow precise localization of individual modules, eliminating the need for external sensors to determine docking positions and thereby significantly improving docking reliability.

In this paper, we propose a two-dimensional deformable lattice MSRR named Rhombot. Each module adopts a rhombus-shaped structure and incorporates a single DoF cable-driven actuation system at its center to enable expansion and contraction along its diagonal. This design provides both compactness and ease of control. Similar to other polyhedral MSRRs, Rhombot modules can be tiled to form a rigid lattice structure when assembled. Alternatively,

each module can be equivalently regarded as a revolute joint connected by rigid links, enabling the formation of serial chains that function as robotic manipulators. This dual nature allows Rhombot to combine the advantages of both lattice-type and chain-type MSRRs. The prototype of Rhombot shown as Fig. 1

This paper is organized as follows. Section II reviews related work on deformable MSRRs. Section III presents the mechanical design and electronic architecture of Rhombot. Section IV analyzes the kinematics and introduces the principle of its morphing motion. Section V validates Rhombot's stable, medium-free reconfiguration capability through a series of experiments, while also demonstrating its deformation and manipulation abilities as supporting functionalities.

## II. RELATED WORK

### A. MSRRs with Lattice Attributes

MSRRs with lattice characteristics have been a major focus of research, as lattice-style designs inherently provide high stiffness and facilitate efficient reconfiguration. According to the survey in [9], 24 out of 39 modular robotic systems can be classified as lattice-type MSRRs. Roombots [20] introduced a design that allows modules to assist each other during reconfiguration, demonstrating strong structural support and versatile reconfiguration capabilities. Similarly, ModQuad [21] and Roboat [22] leverage air and water media, respectively, to achieve cooperative behaviors among modules, thereby achieving capabilities unattainable by individual units. The M-TRAN system [23] was the first to integrate features of both chain-type and lattice-type MSRRs, enabling manipulation capabilities and reconfiguration via wheels mounted on its edges. However, the assistance-based reconfiguration strategy typically requires a larger number of modules and leads to increased control complexity, while other medium-based lattice-type MSRRs exhibit the limitation discussed in Section I.

### B. Deformation MSRRs

Deformable MSRRs employ modules with variable geometry, enabling more versatile reconfiguration strategies compared with rigid lattice- or chain-type systems. A planar modular robotic system based on a six-bar linkage was introduced in [24], allowing each module to move around another while maintaining connectivity throughout the motion. However, actuators were installed at all six vertices, resulting in a high control burden that scales rapidly with the number of modules. In [25], a triangular deformable module was presented, with edges capable of extending and contracting to achieve various triangular configurations. Despite this theoretical versatility, the design cannot realize obtuse triangles, and its reconfiguration strategy has not yet been experimentally demonstrated. Overall, current deformation-based MSRRs highlight the potential of variable-geometry modules but also face challenges such as increased mechanical complexity, scalability issues, and limited demonstrated configurations.

TABLE I  
COMPARISON WITH PREVIOUS MSRRS

MSRR System	DoF	Actuation	Approach	Ports
Metamorphic [24]	3	6	Deformation	6
PARTS [25]	3	3	Deformation	3
M-Blocks [13]	1	1	Pivoting	6
Rhombot (Ours)	1	1	Deformation	4

TABLE II  
PARAMETERS AND SPECIFICATIONS OF RHOMBOT

Item	Definition	Value
$a$	Half of the rhombus side length	140 mm
$b$	Position of the electromagnet installation	70 mm
$\theta$	Folding angle	[45°, 135°]
$T$	Output torque of the servo motor	4.5 kg·cm
$Z_1$	Number of teeth on the output gear	12
$Z_2$	Number of teeth on the input gear	24
$r$	Radius of the winch	5 mm
$F_e$	Standard holding force of the electromagnet	25N

### C. Comparison with previous MSRRs

The Rhombot integrates many functionalities commonly found in advanced lattice-type MSRRs, such as locomotion and inter-module connection/separation. In addition, it inherits certain features of chain-type MSRRs, such as manipulation. However, the primary focus of Rhombot is achieving stable, medium-independent reconfiguration. A comparison with representative MSRR systems is presented in Table I. Compared with Metamorphic robots and PARTS, Rhombot leverages a single degree of freedom (DoF) to simplify reconfiguration control to the greatest extent, while offering a more stable and robust reconfiguration process than M-blocks.

## III. MECHANISM DESIGN AND ELECTRONICS

Rhombot module is composed of multiple parallelogram linkages forming the skeleton, a cable-driven actuation system, four symmetrically distributed connectors, embedded electronics, and additional components necessary for full functionality. The exploded view is shown in Fig. 2(a).

### A. Skeleton and Actuation System

The skeleton, illustrated in Fig. 2(f), consists of multi-parallelogram linkages, which provides the module's fundamental morphing capability and serves as the foundation for integrating other components. With the exception of the central parallelogram structure, which forms a slot-like constraint with an anti-rotation mechanism to restrict diagonal movement and prevent undesired rotation about the center, the entire structure is centrally symmetric. The skeleton is fabricated from carbon fiber plates, providing high stiffness while preserving a compact overall form factor. The geometry is designed to eliminate component interference and ensure that the folding angle  $\theta$  remains within the specified range, with half of the rhombus side length defined as  $a$ .

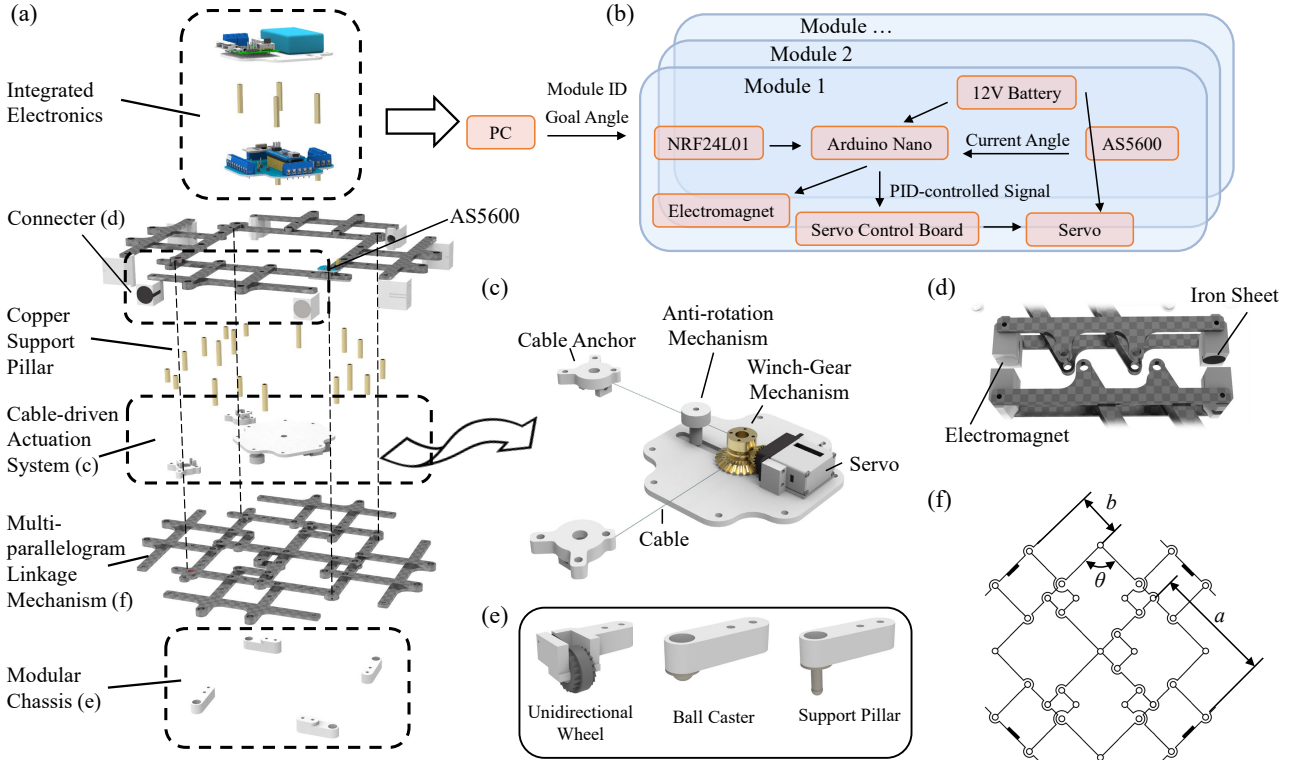


Fig. 2. Mechanism Design and Electronics of the Rhombot. (a) Exploded view of the Rhombot's components. (b) Electronic architecture layout. (c) Actuation system diagram. (d) Pair of hermaphroditic connectors. (e) Modular chassis design. (f) Schematic of the multi-parallelogram linkage mechanism.

The actuation system employs a bevel gear transmission to connect the servo motor to the driving cable, shown as Fig. 2(c). This design allows the servo to be mounted flat, minimizing the vertical dimension of the overall structure, and simultaneously increases actuation torque. The actuation torque  $M_d$  generated between adjacent edges is calculated as:

$$M_d = \frac{T \cdot Z_1}{r \cdot Z_2} \cdot 2a \sin\left(\frac{\theta}{2}\right) \quad (1)$$

where  $T$  is the output torque of the servo,  $Z_1$  and  $Z_2$  are the numbers of teeth of the bevel gear pair, and  $r$  is the radius of the winch.

### B. Connector Design

The connector consists of a normally-on electromagnet and a circular iron plate, shown as Fig. 2(d). The electromagnet actively attracts the iron plate of another connector, creating a hermaphroditic connection. As a normally-on device, the electromagnet maintains its holding force without power, ensuring that modules remain securely connected even during power loss. When a module needs to detach from the robot system, it only deactivates its own electromagnets, while the mating connectors continue to provide resistance torque. The resisting torque is modeled as

$$M_f = F_e \cdot (2a - b) + \varepsilon \quad (2)$$

where  $\varepsilon$  represents the additional frictional resistance at the physical contact surface. To enable single-sided disconnection, the design ensures that  $M_f < M_d$ . Experimental

measurements indicate that  $\varepsilon$  is approximately 0.84 kg·cm. The complete structural design parameters are summarized in Table II.

### C. Electronics

The electronic architecture of the Rhombot module is illustrated in Fig. 2(b). The system integrates a wireless communication module (nRF24L01) for multi-module co-ordination, an Arduino Nano microcontroller, an AS5600 magnetic rotary encoder for measuring the folding angle  $\theta$ , electromagnets for inter-module connections, a servo motor, and a dedicated servo driver board. All electronic components are mounted on custom printed circuit boards (PCBs), resulting in a compact and modular electrical layout. Power is supplied by a 12 V lithium battery with step-down regulators providing the required voltages for each subsystem.

### D. Modular Chassis

The chassis of the Rhombot module adopts a modular design, shown as Fig. 2(e), allowing it to be equipped with unidirectional wheels, ball casters, or support pillars. When equipped with support pillars, the module is anchored to the ground, enabling it to serve as a stable base for the entire system. Ball casters are the default choice for general deployment and are used as the base in all modules presented in this work, providing low-friction omnidirectional support. In contrast, unidirectional wheels enable individual modules to achieve independent mobility but are not considered in the design or experiments of this paper.

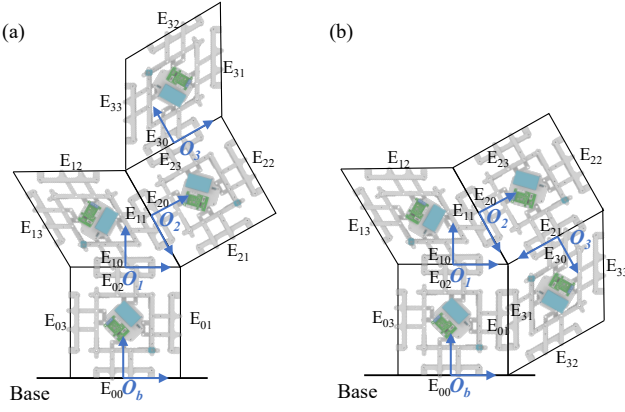


Fig. 3. Two kinematics of Rhombot with configuration representations and reference coordinate frames indicated. (a) Serial connection of four modules. (b) Parallel connection of four modules.

#### IV. MOTION ANALYSIS

##### A. Kinematic Modeling

Since the kinematic system of modular robots varies with changes in the number of modules or their topological arrangement, deriving a single, invariant kinematic model is impractical. A module-based kinematic modeling approach is therefore widely adopted [26], where each kinematic module is denoted as  $M_i (i \in \mathbb{N})$  and connected according to topology, resulting in a kinematic tree.

The Rhombot module is modeled as a two-dimensional quadrilateral. Among its four edges,  $E_0$  is connected either to the parent node or to the base, while the remaining three edges, labeled  $E_1$ ,  $E_2$ , and  $E_3$  in counterclockwise order, serve as interfaces for connecting to other modules. For a given module  $M_i$ , a reference coordinate frame  $\{O_i\}$  is defined at the midpoint of its edge  $E_{i0}$ . The  $y_i$ -axis is oriented toward the geometric center of the module, the  $z_i$ -axis is normal to the plane and directed outward, and the  $x_i$ -axis is determined according to the right-hand rule.

The transformations from the midpoint of  $E_{i0}$  to the midpoints of  $E_{i1}$ ,  $E_{i2}$ , and  $E_{i3}$  are expressed as

$${}^0_1T_i = \begin{bmatrix} R_z(\sigma_i + \pi) & \begin{bmatrix} a + a \cos \sigma_i \\ a \sin \sigma_i \\ 0 \\ 1 \end{bmatrix} \\ 0 & 0 & 0 \end{bmatrix} \quad (3)$$

$${}^0_2T_i = \begin{bmatrix} I_3 & \begin{bmatrix} 2a \cos \sigma_i \\ 2a \sin \sigma_i \\ 0 \\ 1 \end{bmatrix} \\ 0 & 0 & 0 \end{bmatrix} \quad (4)$$

$${}^0_3T_i = \begin{bmatrix} R_z(\sigma_i) & \begin{bmatrix} a - a \cos \sigma_i \\ a \sin \sigma_i \\ 0 \\ 1 \end{bmatrix} \\ 0 & 0 & 0 \end{bmatrix} \quad (5)$$

where  $R_z(\cdot)$  represents a rotation matrix about the  $z$ -axis. The parameter  $\sigma_i$  characterizes the folding–unfolding degree of freedom of module  $M_i$ , corresponding to the interior

##### Algorithm 1: Reconfiguration Strategy

---

```

1 ; /* All operations are performed on
      the module system Ktree */
2 Input: Con_DisconPair
3 InitializeKTree();
4 while Con_DisconPair is not empty do
5   NewCon, NewDiscon ←
      Con_DisconPair.Pop();
6   Edges ← IdentifyEdges(NewCon);
7   Morphpivoting(Edges, NewCon, NewDiscon);
8 end
9 function Morphpivoting(Edges, NewCon,
10   NewDiscon);
11   Connect(Edges, NewCon);
12   Disconnect(NewDiscon);
13   Child ← DetermineChild(NewDiscon);
14   AssignNewParent(Child);
15 end
16 function AssignNewParent(M);
17   foreach Mnear, Mnear-edge in M.conns do
18     Status, Path ← IsConn(Root, Mnear);
19     if Status and M  $\notin$  Path then
20       Connect(M, Mnear, Mnear-edge);
21       UpdateInform(M);
22       RebuildConns();
23     break;
24   end
25 end
26 end

```

---

angle between edges  $E_0$  and  $E_3$ , which can be mapped from  $\theta_i$  based on the connection configuration. Initially,  $\sigma_i = \theta_i$ ; however, after the modules undergo reconfiguration, the reference edge  $E_0$  is redefined, requiring a remapping of  $\sigma_i$ .

When constructing the kinematic tree, one module is always selected as the root module, with its edge  $E_0$  fixed on the base. The coordinate frame  $\{O_0\}$  of the root module is simultaneously defined as the base frame of the entire robotic system, denoted as  $\{O_b\}$ . If a closed-loop structure exists, it can be converted into a tree structure by disconnecting one of the topological connections and introducing additional constraints. Accordingly, the forward kinematics, which is the transformation from the base frame  $\{O_b\}$  to the end-module frame  $\{O_e\}$ , can be expressed as:

$${}^bT = {}^0_1T_0 {}^0_1T_1 {}^0_2T_2 \cdots {}^0_{k_e}T_e \quad (6)$$

where  $K = \{k_0, k_1, k_2, \dots, k_e\}$  denotes the sequence of selected interfaces.

Fig. 3 illustrates the kinematic trees with serial and parallel topologies. In Fig. 3(a), the pose of any module edge can be obtained from (4). In Fig. 3(b), disconnecting  $M_0$ – $M_3$  gives the serial path  $M_0M_1M_2M_3$ , while disconnecting  $M_2$ – $M_3$  gives the path  $M_0M_3$ . Both yield the same center position of  $M_3$ , leading to the basic constraint:

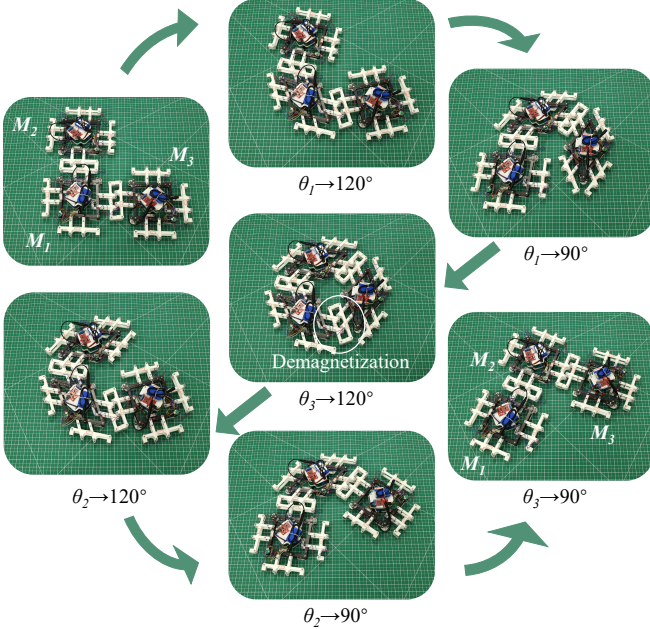


Fig. 4. Demonstration of a morphpivoting operation with three Rhombots.

$${}_2T_0 {}^0T_1 {}^0T_2 {}^0T_3 = {}_1T_0 {}^0T'_3 \quad (7)$$

where  ${}^0T_3$  is the transformation from  $E_0$  to the module center, with  ${}^0T_3 {}^0T_3 = {}^0T_3$ . The  ${}^0T_3$  on both sides of the equation differ because  $\sigma$  is defined differently, and the prime ' distinguishes them.

### B. Reconfiguration Strategy

Based on the above kinematics, we can construct an initial kinematic model for any configuration of the Rhombot and determine the position of each module. Building on this model, we focus on the motion capabilities of the Rhombot. The Rhombot supports most functions of modular self-reconfigurable robots (MSRRs), such as morphing, locomotion, attachment, and detachment. However, these fundamental motions primarily serve as the basis for reconfiguration, which we define as incrementally transitioning the modules from one topological connection state to another. In this work, we introduce morphpivoting as a novel primitive motion that acts as the elemental operation enabling such reconfiguration. Each morphpivoting process consists of four sequential steps: morphing, connection, disconnection, and morphing.

Algorithm 1 presents a systematic strategy for executing multiple *morphpivoting* operations in an orderly manner, based on specified connection and disconnection pairs. First, a topological tree is constructed to represent the modular configuration, initialized according to the geometric positions of the modules and their connectivity relationships (Line 1). For each specified connection pair, the algorithm determines the corresponding module edges involved in the operation and invokes the *Morphpivoting* motion procedure (Lines 2–7). This procedure establishes the required new connec-

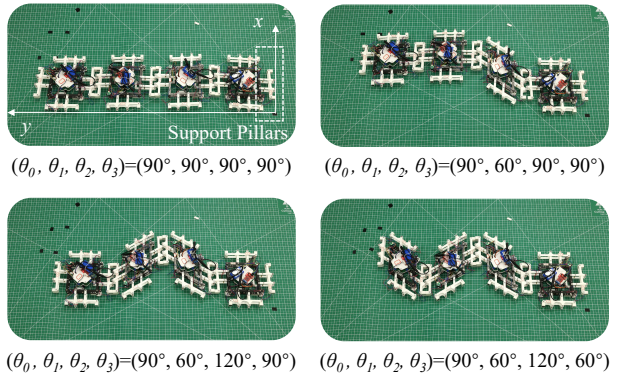


Fig. 5. Kinematic Accuracy of Rhombot's Chain Form.

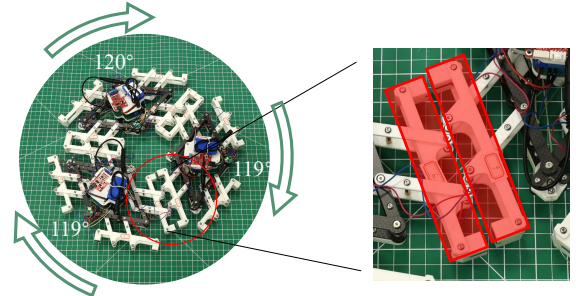


Fig. 6. Docking alignment after multiple morphpivoting.

tion, removes the specified disconnection, and updates the topological tree, with a key focus on inferring parent–child relationships among the affected modules and reassigning parent nodes to ensure a consistent hierarchical structure (Lines 8–13). Subsequently, the *AssignNewParent* function identifies a valid neighboring module to serve as the new parent for the child module, preserving the overall tree connectivity (Lines 14–24). The child module is reattached to this parent through the appropriate edge, and the labeling and connectivity information of all affected modules are updated accordingly. Finally, the *UpdateInform* function recalculates  $E_0$  and remaps  $\sigma$ , which modifies the kinematic tree structure and necessitates its regeneration after each *morphpivoting* operation, as specified in (6).

## V. EXPERIMENTS

### A. Reconfiguration

Fig. 4 illustrates a morphpivoting operation, which consists of morphing, connection, separation, and subsequent morphing between Rhombots. Three modules, denoted as  $M_1$ ,  $M_2$ , and  $M_3$ , are initially configured with  $\theta = 90^\circ$ . Their angles are then sequentially adjusted to  $\theta = 120^\circ$  to form a triangular loop. A new connection is established between  $M_2$  and  $M_3$ , while the connection between  $M_1$  and  $M_3$  is released by demagnetizing the electromagnet. Finally, the angles are sequentially restored to  $\theta = 90^\circ$ .

Due to the limited number of fabricated modules, simulations were conducted to demonstrate the reconfiguration strategy described in Section IV. The transformation process

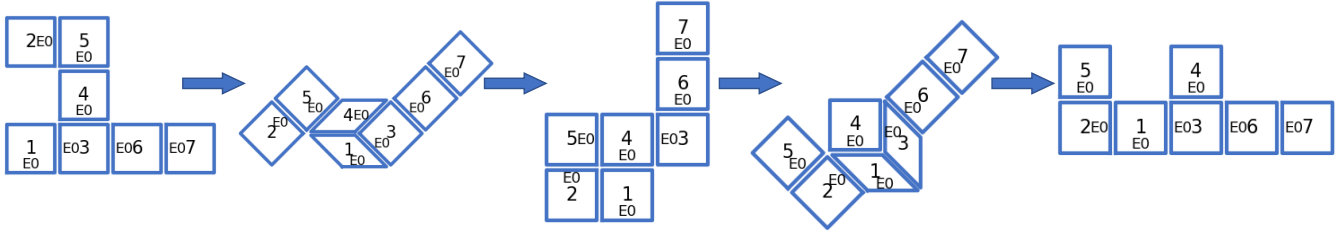


Fig. 7. Simulation of reconfiguration using morphpivoting, transforming the structure from a horizontally placed “μ” shape to a horizontally placed “F” shape.

is shown in Fig. 7, where seven modules arranged in a horizontally placed “μ” configuration are reconfigured into a horizontally placed “F” through multiple morphpivoting operations. The edge indices before and after the transformation are labeled to illustrate the redefinition of edges as the system’s topology changes.

### B. Kinematic Accuracy Evaluation

In a chain configuration, the system is expected to perform manipulator-like operations, since each module can be equivalently modeled as a revolute joint connected by rigid links. The kinematic analysis of the end-effector position was presented in Section IV, and here we experimentally validate the accuracy of the end position on the physical prototype. The experiment was conducted on a green fabric with printed scales to capture the position of each module, with four experimental snapshots shown in Fig. 5. During the experiment, the  $\theta$  values of the modules were adjusted to induce swinging motions of the chain structure. For each configuration, the intersection point of  $E_1$  and  $E_2$  on the end module was measured as the ground-truth position, while the theoretical position was obtained through kinematic analysis. A comparison between the measured and calculated positions shows an RMSE of approximately 4.77 mm along the  $x$ -axis and 14.96 mm along the  $y$ -axis. The larger error in the  $y$ -direction is attributed to longitudinal friction that hindered extension along this axis, despite the use of ball casters.

### C. Docking Accuracy Evaluation

To validate the stability of the reconfiguration process, the procedure illustrated in Fig. 4 was repeated for seven consecutive trials. In the final morphpivoting step, the  $\theta$  angles of modules  $M_1$  and  $M_3$  were set to 119° to bring them into close proximity for docking observation, as shown in Fig. 6. The red-highlighted region indicates the relative offset between the two connectors, which remains within the acceptable tolerance.

## VI. DISCUSSION

In practical implementation, imperfect cable tensioning and variations in the diagonal length during the morphing process result in a slight offset between the servo strokes in the forward (increasing  $\theta$ ) and reverse (decreasing  $\theta$ ) rotations, as illustrated in Fig. 8. This offset corresponds to approximately 1500 encoder counts, or about 131° given

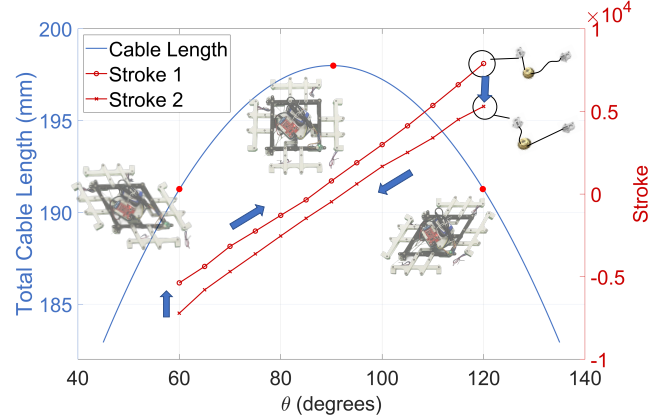


Fig. 8. Total cable length and servo strokes in forward and reverse directions plotted against the folding angle  $\theta$ .

a resolution of 4095, and is unavoidable near the end ranges of motion. In the physical prototype, two springs were incorporated to mitigate cable slack, ensuring that this issue does not fundamentally affect system performance. For future improvements, an irregular winch design could be considered to further reduce this effect.

## VII. CONCLUSION

This paper presents a novel lattice-based MSRR, Rhombot, which demonstrates stable and medium-independent reconfiguration capabilities. Rhombot is driven by a single servo, offering high controllability for individual modules while enabling advanced MSRR functionalities such as morphing, connection/disconnection, and more. Its lattice structure allows for planar tiling, achieving the high rigidity inherent in lattice-based MSRRs. At the same time, simplifying each module to a rotational pair and linkage provides the flexibility characteristic of chain-based MSRRs. The reconfiguration capabilities and docking precision of the Rhombot system were experimentally validated.

Several avenues for future research exist. For instance, the modular chassis could be replaced with unidirectional wheel, to investigate locomotion for individual modules and synchronized movement for multi-module, such as snake-like configurations. In terms of reconfiguration planning, a critical next step is the development of an autonomous algorithm that uses the morphpivoting motion as a primitive. Such an algorithm would generate optimal action sequences,

overcoming the current limitation of manually specified connection/disconnection pairs. This will be fundamental to achieving large-scale and fully autonomous applications for the Rhombot system.

## REFERENCES

- [1] G. Liang, H. Luo, M. Li, H. Qian, and T. L. Lam, "Freebot: A freeform modular self-reconfigurable robot with arbitrary connection point-design and implementation," in *2020 IEEE/RSJ International Conference on Intelligent Robots and Systems (IROS)*. IEEE, 2020, pp. 6506–6513.
- [2] Y. Tu, G. Liang, and T. L. Lam, "FreeSN: A freeform strut-node structured modular self-reconfigurable robot-design and implementation," in *2022 International Conference on Robotics and Automation (ICRA)*. IEEE, 2022, pp. 4239–4245.
- [3] C. H. Belke and J. Paik, "Mori: a modular origami robot," *IEEE/ASME Transactions on Mechatronics*, vol. 22, no. 5, pp. 2153–2164, 2017.
- [4] A. Spinos, D. Carroll, T. Kientz, and M. Yim, "Variable topology truss: Design and analysis," in *2017 IEEE/RSJ International Conference on Intelligent Robots and Systems (IROS)*. IEEE, 2017, pp. 2717–2722.
- [5] A. Castano, W.-M. Shen, and P. Will, "CONRO: Towards deployable robots with inter-robots metamorphic capabilities," *Autonomous Robots*, vol. 8, pp. 309–324, 2000.
- [6] P. Swissler and M. Rubenstein, "Fireant: a modular robot with full-body continuous docks," in *2018 IEEE International Conference on Robotics and Automation (ICRA)*. IEEE, 2018, pp. 6812–6817.
- [7] D. Zhao, H. Luo, Y. Tu, C. Meng, and T. L. Lam, "Snail-inspired robotic swarms: a hybrid connector drives collective adaptation in unstructured outdoor environments," *Nature Communications*, vol. 15, no. 1, p. 3647, 2024.
- [8] J. Zheng, G. Dai, B. He, Z. Mu, Z. Meng, T. Zhang, W. Zhi, and D. Fan, "Rs-modcubes: Self-reconfigurable, scalable, modular cubic robots for underwater operations," *IEEE Robotics and Automation Letters*, 2025.
- [9] G. Liang, D. Wu, Y. Tu, and T. L. Lam, "Decoding modular reconfigurable robots: A survey on mechanisms and design," *arXiv preprint arXiv:2310.09743*, 2023.
- [10] C. Liu, Q. Lin, H. Kim, and M. Yim, "SMORES-EP, a modular robot with parallel self-assembly," *Autonomous Robots*, vol. 47, no. 2, pp. 211–228, 2023.
- [11] A. Spröwitz, R. Moeckel, M. Vespignani, S. Bonardi, and A. J. Ijspeert, "Roombots: A hardware perspective on 3d self-reconfiguration and locomotion with a homogeneous modular robot," *Robotics and Autonomous Systems*, vol. 62, no. 7, pp. 1016–1033, 2014.
- [12] L. Zhao, Y. Wu, W. Yan, W. Zhan, X. Huang, J. Booth, A. Mehta, K. Bekris, R. Kramer-Bottiglio, and D. Balkcom, "Starblocks: Soft actuated self-connecting blocks for building deformable lattice structures," *IEEE Robotics and Automation Letters*, vol. 8, no. 8, pp. 4521–4528, 2023.
- [13] J. W. Romanishin, K. Gilpin, and D. Rus, "M-blocks: Momentum-driven, magnetic modular robots," in *2013 IEEE/RSJ International Conference on Intelligent Robots and Systems*. IEEE, 2013, pp. 4288–4295.
- [14] J. W. Romanishin, K. Gilpin, S. Claić, and D. Rus, "3d m-blocks: Self-reconfiguring robots capable of locomotion via pivoting in three dimensions," in *2015 IEEE International Conference on Robotics and Automation (ICRA)*. IEEE, 2015, pp. 1925–1932.
- [15] M. Pieber, R. Neurauter, and J. Gerstmayr, "An adaptive robot for building in-plane programmable structures," in *2018 IEEE/RSJ International Conference on Intelligent Robots and Systems (IROS)*. IEEE, 2018, pp. 1–9.
- [16] B. Piranda and J. Bourgeois, "Datom: A deformable modular robot for building self-reconfigurable programmable matter," in *International Symposium Distributed Autonomous Robotic Systems*. Springer, 2021, pp. 70–81.
- [17] Y. Qin, L. Ting, C. Saven, Y. Amemiya, M. Tanis, R. D. Kamien, and C. Sung, "Trussbot: Modeling, design, and control of a compliant, helical truss of tetrahedral modules," in *2022 International Conference on Robotics and Automation (ICRA)*. IEEE, 2022, pp. 4218–4224.
- [18] A. Lyder, R. F. M. Garcia, and K. Stoy, "Mechanical design of odin, an extendable heterogeneous deformable modular robot," in *2008 IEEE/RSJ International Conference on Intelligent Robots and Systems*. Ieee, 2008, pp. 883–888.
- [19] N. S. Usevitch, Z. M. Hammond, M. Schwager, A. M. Okamura, E. W. Hawkes, and S. Follmer, "An untethered isoperimetric soft robot," *Science Robotics*, vol. 5, no. 40, p. eaaz0492, 2020.
- [20] A. Sproewitz, A. Billard, P. Dillenbourg, and A. J. Ijspeert, "Roombots-mechanical design of self-reconfiguring modular robots for adaptive furniture," in *2009 IEEE international conference on robotics and automation*. IEEE, 2009, pp. 4259–4264.
- [21] D. Saldana, B. Gabrich, G. Li, M. Yim, and V. Kumar, "ModQuad: The flying modular structure that self-assembles in midair," in *2018 IEEE International Conference on Robotics and Automation (ICRA)*. IEEE, 2018, pp. 691–698.
- [22] W. Wang, B. Gheneti, L. A. Mateos, F. Duarte, C. Ratti, and D. Rus, "Roboat: An autonomous surface vehicle for urban waterways," in *2019 IEEE/RSJ International Conference on Intelligent Robots and Systems (IROS)*. IEEE, 2019, pp. 6340–6347.
- [23] H. Kurokawa, K. Tomita, A. Kamimura, S. Kokaji, T. Hasuo, and S. Murata, "Distributed self-reconfiguration of m-tran iii modular robotic system," *The International Journal of Robotics Research*, vol. 27, no. 3-4, pp. 373–386, 2008.
- [24] A. Pamecha, I. Ebert-Uphoff, and G. S. Chirikjian, "Useful metrics for modular robot motion planning," *IEEE Transactions on Robotics and Automation*, vol. 13, no. 4, pp. 531–545, 2002.
- [25] M. Gerbl, M. Pieber, E. Ulrich, and J. Gerstmayr, "PARTS—a 2d self-reconfigurable programmable mechanical structure," *Robotics*, vol. 13, no. 5, p. 77, 2024.
- [26] Y. Tu, G. Liang, D. Wu, X. Li, and T. L. Lam, "Locomotion and self-reconfiguration autonomy for spherical freeform modular robots," *The International Journal of Robotics Research*, p. 02783649251360360, 2025.